Capillary filling dynamics of viscoelastic fluids

Aditya Bandopadhyay,[1] Uddipta Ghosh,[2] and Suman Chakraborty[1,2,*]
[1]*Advanced Technology Development Center, Indian Institute of Technology Kharagpur, Kharagpur-721302, India*
[2]*Department of Mechanical Engineering, Indian Institute of Technology Kharagpur, Kharagpur-721302, India*
(Received 17 December 2013; published 29 May 2014)

We consider the filling of a capillary by a viscoelastic fluid described by the Phan-Thien–Tanner (PTT) constitutive behavior. By considering both vertical capillary filling and horizontal capillary filling, we demarcate the role played by gravity and fluid rheology towards long-time oscillations in the capillary penetration depth. We also consider the isothermal filling of the capillary for a closed channel and thus bring out the fundamental differences in the nature of capillary filling for PTT and Newtonian fluids for closed channels in comparison to open channels. Through a scaling analysis, we highlight a distinct viscoelastic regime in the horizontal capillary filling which is in contrast to the Washburn scaling seen in the case of Newtonian fluids. Such an analysis with a very general constitutive behavior is therefore expected to shed light on many areas of microfluidics which focus on biofluids that are often well described by the PTT constitutive behavior.

DOI: 10.1103/PhysRevE.89.053024 PACS number(s): 47.61.−k

I. INTRODUCTION

In recent times, there has been a focus on development of "lab-on-a-chip" (LOC) devices which facilitate fast and reliable on-site analysis with extremely small quantities of samples and reagents [1]. A very fundamental design feature of such LOC devices is the pumping (transport) of liquids (either reagents or samples). Depending on the type of liquid, it may be driven by several mechanisms such as the mechanical pressure pump [1,2], electro-osmosis [3,4], thermal pumps [5–7], etc. As is evident, such *actively* driven devices necessitate an external source of power and intrusion into the flow field which are likely to render the LOC device complex and prone to failure. As an alternate to such active devices, one may have *passive* pumping wherein surface tension, in conjunction with the high surface area to volume ratio, can be exploited to initiate the flow by advantageously tuning surface properties such as wettability and the geometric parameters such as the introduction of micro- or nanopillars [8–15]. Such passive pumping does not rely on any external sources for activation and hence can work autonomously.

Recognizing the importance of such a process, several studies have been reported on the analysis of the filling of capillaries which cover not only numerical [16–21], experimental [22–24], and analytical modeling [3,4,10,25–28], but also evidence from molecular dynamics [29–31]. Differences between the capillary filling in open and closed channels has also been a topic of interest in recent times [32,33]. While such theoretical and numerical considerations have improved our understanding of the basic regimes of flow, most of these analyses remain limited by the fact that the fluid is considered to be Newtonian in nature. From a point of view of applications in LOC devices (which typically handle biological fluids), it is of paramount importance to consider the appropriate deviation of the fluid from Newtonian behavior. To the authors' knowledge there are very few works pertaining to the filling of capillaries by non-Newtonian fluids, most of which deal with power-law constitutive behavior [34–36] or simple viscoelastic models [37].

From a point of view of modeling, rheologically, the Phan-Thien–Tanner (PTT) model [38] which models viscoelastic fluids is able to encompass a wide variety of non-Newtonian fluids ranging from polymer solutions to complex biofluids such as blood [35,39–42]. Several other constitutive behaviors can be modeled as limiting cases of the PTT model [43] and hence, the analysis of a PTT fluid would help in advancing the current understanding of capillary imbibition.

Here we consider the filling of a capillary by a PTT fluid. We first derive a governing equation by considering a reduced order model. By assuming a fully developed velocity profile, we obtain the shear stress acting on the liquid column. In the present analysis, we have accounted for both horizontal and vertical filling. We also derive the governing equation for isothermal capillary filling in the case where the capillary is closed. We demonstrate the differences between capillary filling for a PTT fluid and a Newtonian fluid by considering first the numerical solution for the governing differential equations and then by a scaling estimate. Through our scaling estimates, we obtain an intermediate regime between the inertial capillary regime and the Washburn regime which is a characteristic of the PTT fluid. In addition to this, we also linearize the pertinent governing equation around the Jurin (equilibrium) height. From this, we predict the onset of an oscillatory behavior in the case of near-Newtonian fluids for vertical filling of both open and closed capillaries.

II. MATHEMATICAL FORMULATION

As a physical system for the present analysis, we chose a capillary, consisting of two parallel plates, kept at a distance of $2H$. In the present study we will consider both vertical and horizontal orientations of the capillary. We will further consider the cases of a closed capillary, where one end of the channel is blocked, with trapped air being present inside it. The length of the capillary is taken as L, which is much larger than the spacing between the plates ($L \gg 2H$). In cases of an open capillary, we can make $L \to \infty$ to virtually render the effect of the entrapped gas negligible. We will consider a

*suman@mech.iitkgp.ernet.in

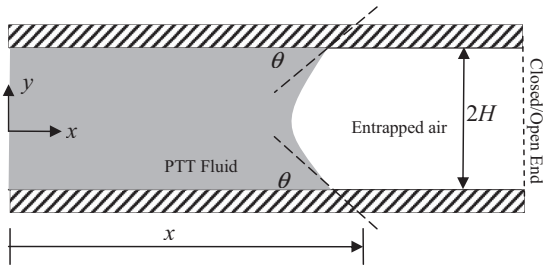

FIG. 1. Schematic of the problem. The PTT fluid front penetrates into a distance x into a capillary with either closed or open end. The contact angle between the fluid and the wall is θ. The channel height is $2H$.

case where the capillary is being filled by a pure viscoelastic fluid, demonstrating a rheological behavior described by the linear Phan-Thien–Tanner model (PTT) [44]. The density of the fluid is taken as ρ, the equilibrium contact angle at the fluid-solid-gas interface is taken to be θ, the viscosity of the fluid is denoted by η, while the surface tension at the fluid-gas interface is taken as γ_s. For simplicity we will only consider cases where the contact angle at the solid-liquid-gas interface remains constant. Since, in the present analysis we are considering a closed capillary, we have to take into account the effects of entrapped air inside the channel. Again, in an effort to make the analysis algebraically simple, yet without sacrificing the essential physics, we consider the entrapped gas to be an ideal gas. We will track the pressure volume changes of the gas by applying Boyle's law, supposing the process of capillary filling to be isothermal in nature and neglecting the heat generation from viscous dissipation. In the present analysis, we will employ a lumped model, in order to bring out the essential features of capillary dynamics, when the filling fluid is viscoelastic in nature (PTT model). A schematic of the system under consideration has been depicted in Fig. 1. As evident from the figure, we place the origin at the channel centerline, where the x axis runs along the axial direction and the y axis is the cross-channel coordinate.

We start by deriving the velocity profile of a PTT fluid, under the action of a steady pressure gradient in a parallel plate channel, with an assumption that the flow is fully developed. We follow the considerations by Oliveira and Pinho [44] in deriving the necessary expressions for the stress at the walls. The constitutive relation for the PTT model is given by [44]

$$f(\mathrm{Tr}\,(\tau))\tau + \lambda\tau^{\nabla} = 2\eta D, \tag{1}$$

where $\mathrm{Tr}(A)$ denotes the trace of a tensor A, f signifies the extent of nonlinearity in the PTT model, λ is the characteristic relaxation time, η is the dynamic viscosity of the fluid, D is the strain rate tensor, and τ^{∇} is the Gordon-Schowalter derivative given as $\tau^{\nabla} = \frac{D\tau}{Dt} - \tau\cdot\nabla\mathbf{u} - \nabla\mathbf{u}^{T}\cdot\tau$, where τ is the stress tensor, $\mathbf{u}$ is the velocity field, and T in the superscript denotes the transpose of a tensor. In the case of linear PTT model, the function f is given by $f(\mathrm{Tr}\,(\tau)) = 1 + \frac{\varepsilon\lambda}{\eta}\mathrm{Tr}\,(\tau)$, where ε is the elongation parameter. In contrast to the linear PTT model, we may also have the exponential PTT model which is given by $f(\mathrm{Tr}\,(\tau)) = \exp\left(\frac{\varepsilon\lambda}{\eta}\mathrm{Tr}\,(\tau)\right)$. It is quite obvious from the above discussion that under the limiting cases of small values of $\frac{\varepsilon\lambda}{\eta}\mathrm{Tr}\,(\tau)$, the exponential or the nonlinear PTT model may be approximated by the linear PTT model. Considering a fully developed flow (please refer to the Appendix for a justification of the assumption of a fully developed steady state flow) of a PTT fluid, the stress-strain relations take the form [44]

$$f\,(\tau_{kk})\,\tau_{xx} = 2\lambda u_{,y}\tau_{xy}, \tag{2a}$$

$$f\,(\tau_{kk})\,\tau_{yy} = 0, \tag{2b}$$

$$f\,(\tau_{kk})\,\tau_{xy} = \eta u_{,y} + \eta\tau_{yy}u_{,y}. \tag{2c}$$

Here, $\tau_{kk} = \tau_{xx} + \tau_{yy}$. Therefore, from Eq. (2b) we have $\tau_{yy} = 0$ and hence $\tau_{kk} = \tau_{xx}$. Combining Eqs. (2a) and (2c), we finally get

$$\tau_{xx} = \frac{2\lambda}{\eta}\tau_{xy}^{2}. \tag{3}$$

With these considerations, the Cauchy's equation of motion can be written as

$$0 = -P_{,x} + \tau_{xy,y}, \tag{4}$$

where the notation $A_{,x}$ denotes the partial derivative of A with respect to x. We can easily solve for τ_{xy} from Eq. (4) to obtain $\tau_{xy} = P_{,x}y$. Substituting this in Eq. (3), we obtain $\tau_{xx} = \frac{2\lambda}{\eta}P_{,x}^{2}y^{2}$. Note that for deriving the solution for τ_{xy} we have used the symmetry condition at the channel centerline. The strain rate ($\dot{\gamma}$) can be defined as [from Eq. (2c)]

$$\dot{\gamma} \equiv \frac{du}{dy} = \frac{1}{\eta}f\,(\tau_{xx})\,\tau_{xy} = \frac{1}{\eta}P_{,x}y\;f\left(\frac{2\lambda}{\eta}(P_{,x}y)^{2}\right). \tag{5}$$

For a linear PTT model, the velocity profile can be deduced by simply integrating Eq. (5) to obtain

$$u = -\frac{1}{2\eta}H^{2}P_{,x}\left\{1 - \left(\frac{y}{H}\right)^{2} + \frac{\varepsilon\lambda^{2}P_{,x}^{2}H^{2}}{\eta^{2}}\left[1 - \left(\frac{y}{H}\right)^{4}\right]\right\}. \tag{6}$$

For nondimensionalizing the velocity profile we adapt the following reference values: $u_{\mathrm{ref}} = -\frac{1}{2\eta}H^{2}P_{,x}$; $L_{\mathrm{ref}} = H$. We further define $\sigma = \frac{4\varepsilon\lambda^{2}}{H^{2}}$. Hence, the velocity profile can be represented in terms of these variables in the following way:

$$u = u_{\mathrm{ref}}\left[(1-\bar{y}^{2}) + \sigma u_{\mathrm{ref}}^{2}(1-\bar{y}^{4})\right]. \tag{7}$$

We now obtain the average velocity by integrating Eq. (7) across the channel. The average velocity is given by

$$\bar{u} = \frac{u_{\mathrm{ref}}}{2}\left[\frac{4}{3} + \sigma u_{\mathrm{ref}}^{2}\frac{8}{5}\right]. \tag{8}$$

As mentioned earlier, in the present analysis, we will follow a reduced order model [22,28,32,33,45–48] for capillary filling dynamics. Therefore, in an effort to evaluate the viscous forces, we will replace the average velocity with the velocity of the capillary front; i.e., $\frac{dx}{dt} = \bar{u}$ and x is the position of the capillary front at time t. Towards this, we first attempt to obtain an expression for u_{ref} in terms of the average velocity. This is achieved from a simple solution of

the cubic equation (8), which reads

$$u_{\rm ref} = \frac{\left[\left(135\bar{u} + 5\sqrt{\frac{40+729\bar{u}^2\sigma}{\sigma}}\right)\sigma^2\right]^{1/3}}{6\sigma} - \frac{5}{3\left[\left(135\bar{u} + 5\sqrt{\frac{40+729\bar{u}^2\sigma}{\sigma}}\right)\sigma^2\right]^{1/3}}. \quad (9)$$

Note that the other two roots of Eq. (8) are complex; hence we discard them. The viscous stress on the walls is then given by

$$\tau_{xy}|_{-H} = \tau_{xy}|_{H} = \frac{2\eta}{H}u_{\rm ref}. \quad (10)$$

Combining Eqs. (9) and (10), one can express the total viscous resistance to the motion of the capillary front in the following way:

$$F_{\rm visc} = 2\tau_{xy}x = \frac{4\eta x}{H}u_{\rm ref}. \quad (11)$$

Here, $u_{\rm ref}$ is given by the expression (9). Now, we move towards the equation governing the capillary dynamics, which can be expressed as a force balance given as

$$\frac{d}{dt}\left(2\rho H x\frac{dx}{dt}\right) = F_{\rm st} - F_{\rm visc} - F_{\rm grav} - F_{\rm gas}. \quad (12)$$

In Eq. (12), $F_{\rm st}$, $F_{\rm visc}$, $F_{\rm grav}$, and $F_{\rm gas}$, respectively, denote surface tension force (the driving force), viscous resistance, gravitational force, and retarding force exerted by the entrapped gas in a closed capillary. Note that Eq. (12) has been written for unit depth of the capillary in the z direction. The surface tension force is given by

$$F_{\rm st} = 2\gamma_s\cos\theta. \quad (13)$$

The viscous force has already been expressed in Eq. (11). The gravitational force is given by

$$F_{\rm grav} = 2\rho g H x. \quad (14)$$

$F_{\rm gas}$, i.e., the force exerted by the entrapped gas in the capillary (closed) is given by [33]

$$F_{\rm gas} = 2H\left(p_t - p_0\right). \quad (15)$$

In Eq. (15), p_t is the pressure of the entrapped gas and p_0 is the atmospheric pressure. The pressure p_t of the entrapped gas can be found out from Boyle's law (assuming the gas to behave as an ideal gas, as stated earlier), which reads

$$2p_t\left(L - x\right)H = 2p_0 LH. \quad (16)$$

Therefore, $F_{\rm gas}$ can be expressed as

$$F_{\rm gas} = 2p_0 H\left(\frac{x}{L-x}\right). \quad (17)$$

Combining Eqs. (12)–(17), the governing equation for capillary motion can be expressed in the following way:

$$\frac{d}{dt}\left[(2\rho Hx)\frac{dx}{dt}\right] = 2\gamma_s\cos\theta - \frac{4\eta x}{H}u_{\rm ref} - 2\rho g H x - 2p_0 H\left(\frac{x}{L-x}\right). \quad (18)$$

For nondimensionalizing equation (18), we adapt the following scheme: $\bar{x} = x/H$ and $\bar{t} = t/t_{\rm ref}$, where $t_{\rm ref}$ is given by $t_{\rm ref} = \sqrt{\rho H^3/\gamma_s}$. Enforcing this scheme in Eq. (18), the final nondimensional equation can be expressed as

$$\frac{d}{d\bar{t}}\left[(\bar{x})\frac{d\bar{x}}{d\bar{t}}\right] = \cos\theta - \frac{2\eta\beta\bar{x}}{\gamma_s}\bar{h}\left(\frac{d\bar{x}}{d\bar{t}}\right) - \frac{g\rho H^2}{\gamma_s}\bar{x} - \xi\left(\frac{\bar{x}}{\bar{L}-\bar{x}}\right). \quad (19)$$

In Eq. (19), $\beta = \sqrt{\frac{\gamma_s}{\rho H}}$, $\xi = p_0 H/\gamma_s$, and

$$\bar{h}\left(\frac{d\bar{x}}{d\bar{t}}\right) = \left(\frac{1}{6\left(\delta\right)^{1/3}}\left[135\frac{d\bar{x}}{d\bar{t}} + 5\sqrt{\frac{40+729\left(\frac{d\bar{x}}{d\bar{t}}\right)^2\delta}{\delta}}\right]^{1/3} - \frac{1}{\left(\delta\right)^{2/3}}\left\{\frac{5/3}{\left[135\frac{d\bar{x}}{d\bar{t}} + 5\sqrt{\frac{40+729\left(\frac{d\bar{x}}{d\bar{t}}\right)^2\delta}{\delta}}\right]^{1/3}}\right\}\right). \quad (20)$$

In Eq. (20), $\delta = \beta^2\sigma$. Note that for horizontal orientation of the capillary, the gravitation force is absent, which can be represented by enforcing $g = 0$. For the cases of open capillary, where no entrapped gases are present, we can make either $\xi = 0$ or $\bar{L} \to \infty$ to render $F_{\rm gas}$ zero. In the next section we will highlight the effects of these forces on the motion of the capillary in detail.

III. RESULTS AND DISCUSSIONS

Reiterating the focus of this work, in this section we attempt to discuss the implications of fluid rheology on capillary filling and compare them with the Newtonian counterparts. Towards this, we note that the fluid rheology, in the case of a PTT fluid, is most aptly described by the elongational parameter (ε) and the relaxation time (λ), apart from the other dynamical properties such as viscosity (η) and density (ρ). Therefore, our main aim will be to investigate the effects of these two properties (ε and λ) on the capillary dynamics of a PTT fluid. A close review of Eqs. (19) and (20) also suggests that apart from the viscosity η, another parameter which shapes the viscous force is σ which is expressed as $\sigma = \frac{4\varepsilon\lambda^2}{H^2}$, combining the influences of the elongational parameter and relaxation time. We will further investigate the effects of gravity and entrapped air on the motion of the capillary front in the case of a PTT fluid, by looking into the motion of the same with and without these forces. Later in this section, we will also attempt to linearize the governing equation (19) in an effort to investigate the motion of the front near the Jurin height (the so-called long-time solution) and in particular focus on the possibilities of capillary front oscillation. We further attempt to bring forward a scaling analysis of the capillary front motion, in order to highlight the effects of various forces in different regimes for a PTT fluid. Throughout the analysis, we have taken the following parameters to be constants (liquid water), $\eta = 10^{-3}$ Pa s, $p_0 = 101.32$ kPa, $\rho = 1000$ kg/m^3, $g = 9.81$ m/s^2, $\gamma_s = 0.072$ N/m, and a contact angle of 0° (perfectly wetting). We also mention

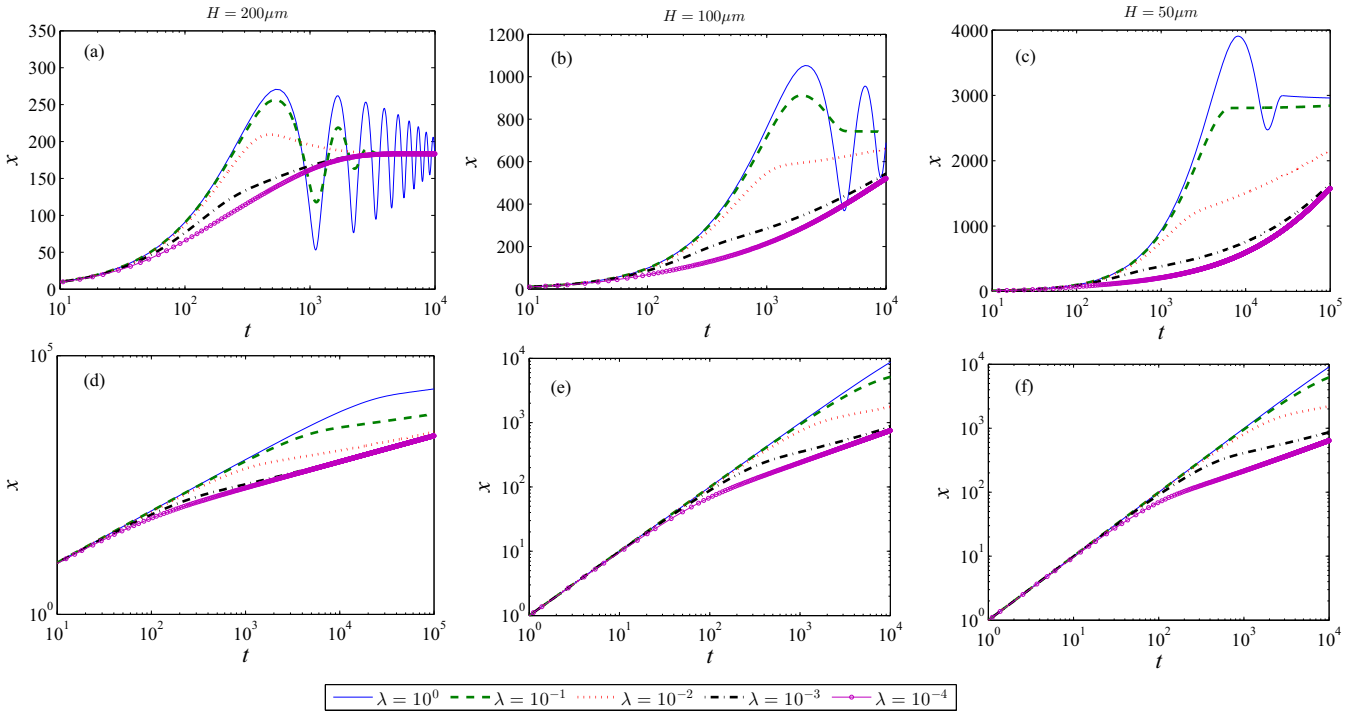

FIG. 2. (Color online) Capillary penetration distance as a function of time for different PTT fluid parameters. The subplots (a)–(c) represent the cases for open vertical filling in channels having $H = 200$, 100, and 50 μm, respectively. The subplots (d)–(f) represent the cases for open horizontal filling in channels having $H = 200$, 100, and 50 μm, respectively. The elongation parameter is fixed at $\varepsilon = 0.1$ in all the subplots.

that for ease of representation we will drop the bar signs from the nondimensional variables in the subsequent sections. However, all the values of the dimensional parameters have been mentioned along with proper units in the forthcoming discussions.

A. Filling dynamics: Open channel

We start our discussion with Fig. 2, where we investigate the capillary penetration distance as a function of time for filling in open capillaries. The first row of plots depicts the filling dynamics for open vertical capillaries of different channel heights (200, 100, and 50 microns) whereas the second row depicts the filling dynamics for open horizontal capillaries of different channel heights (200, 100, and 50 microns). The relaxation time is varied in each case from 1 to 10^{-4} s. It can be observed that regardless of the capillary orientation, the initial regime of filling is largely independent of the PTT rheology as apparent from all the subplots. This initial regime is the inertial regime where the capillary filling is driven by the balance of the surface tension forces and the inertial forces [45]. At longer times however, the capillary filling is mainly dictated by the fluid rheology. In the case of vertical filling, it can be seen that a larger relaxation time leads to large amplitude oscillations near the Jurin height. As the relaxation time decreases (i.e., behavior tends to that of a Newtonian fluid), the amplitudes of the oscillations decrease. The aforementioned high amplitude oscillations of the capillary front may be attributed to the enhanced average velocity of the front on account of the parameter $\sigma = \frac{4\varepsilon\lambda^2}{H^2}$ as seen in Eq. (7). As the channel height is decreased, it is seen that with properties remaining the same, the oscillations begin to disappear even for large relaxation times. This can be attributed to the fact that as we decrease the channel height (H), the viscous forces get stronger ($F_{\text{visc}} \sim \beta \sim H^{-1/2}$) and hence are able to prevent the overshooting of the capillary front's movement. For all the cases, the filling distance is higher for fluids with larger relaxation times, although the equilibrium height (or the Jurin height) remains the same for all the fluids, in cases of vertical capillary filling. Similar trends can be seen in the case of capillary filling in open horizontal channels. The initial filling regime is not rheologically driven. However, the long-time dynamics is clearly rheologically driven as evident from a larger filling distance for the PTT fluid having a larger relaxation time. We will elaborate more on the different regimes of filling at small times and long times in a more qualitative way in the subsequent discussions.

In Fig. 3, we depict the capillary penetration distance as a function of time for different elongation parameters. Once again, the top row depicts the capillary filling in open vertical channels and the bottom row depicts the capillary filling in open horizontal channels. The three columns are representative of different channel heights (200, 100, and 50 microns, respectively). As with the case in Fig. 2, the influence of channel height is apparent in inducing the long-time oscillations in open vertical channels. As the channel height is increased, the long-time oscillations die down and become largely damped, a facet which we shall study in great detail in the later subsections. We further observe that larger values of the elongational parameter lead to oscillations of the capillary front near the Jurin height, as evident from Figs. 3(a)–3(c). For the case of horizontal capillaries, the filling is much faster for fluids with larger elongation parameter values. As mentioned in the previous section, an increase in the values

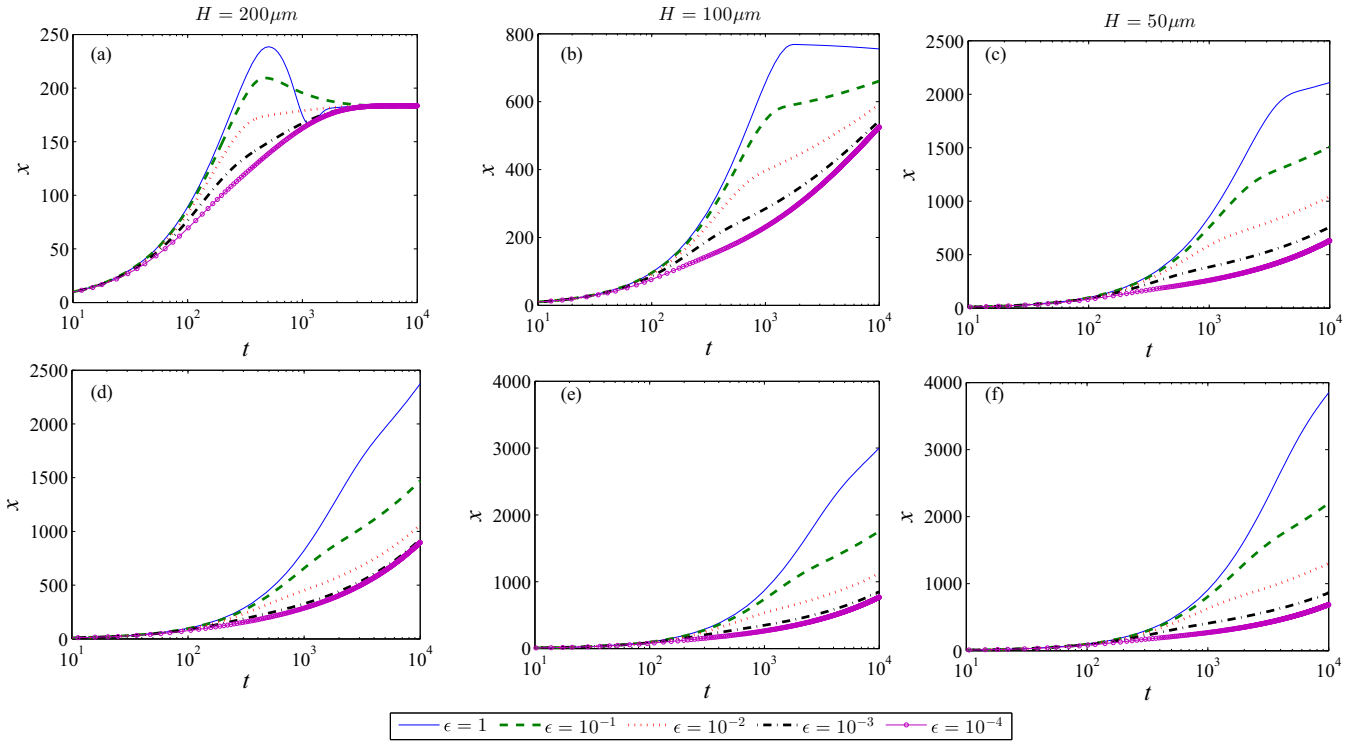

FIG. 3. (Color online) Capillary penetration distance as a function of time for different PTT fluid parameters. The subplots (a)–(c) represent the cases for open vertical filling in channels having $H = 200$, 100, and 50 μm, respectively. The subplots (d)–(f) represent the cases for open horizontal filling in channels having $H = 200$, 100, and 50 μm, respectively. The relaxation time is fixed at $\lambda = 0.01$ s in all the subplots.

of either λ or ε results in an increase in σ, leading to significant departure from simple Newtonian behavior. Since σ varies with $\sim\lambda^2$ and $\sim\varepsilon$, the effect of increasing λ or the relaxation time is more drastic than varying ε, as evident from Figs. 2 and 3. Therefore in essence, departure from Newtonian behavior, quantified by the variation of σ, implicates faster filling and presence of oscillations near the equilibrium height, with the other dynamical properties remaining the same as Newtonian models.

B. Filling dynamics: Closed channel

In order to assess the implications of a closed channel on capillary filling, we consider the variation of the filling distance as a function of time for PTT fluid ($\varepsilon = 0.1$, $\lambda = 0.01$ s) and Newtonian fluid, in a closed vertical channel, as depicted in Fig. 4. It can be seen that as compared to the filling in open channels, the capillary penetration distance for both PTT and Newtonian fluids in closed channels is drastically attenuated as attributable to the added filling dependent pressure which acts as a retarding force on the capillary front. Interestingly, both Newtonian and PTT fluids undergo oscillations near the equilibrium height, when entrapped air is present inside the channel, i.e., the channel is closed. The amplitudes of oscillations are higher for PTT fluids as compared to Newtonian ones, whereas the frequency of oscillation for both remains almost the same. Therefore, a closed capillary triggers oscillations more quickly, as compared to an open channel. For all the filling properties, the long-time behavior is unaltered by the nature of the rheology owing to the lower strain rates near the Jurin (equilibrium) height.

In view of the previous discussion regarding filling in closed vertical channels, we consider capillary filling in closed horizontal channels in Fig. 5. We consider a PTT fluid of the same parameters as that of the previous case and compare it against the Newtonian counterpart. The channel height is 200 microns and $\bar{L}$ is 1000. As expected, the filling in the case of closed capillaries yields a faster convergence to the equilibrium position with early oscillations induced

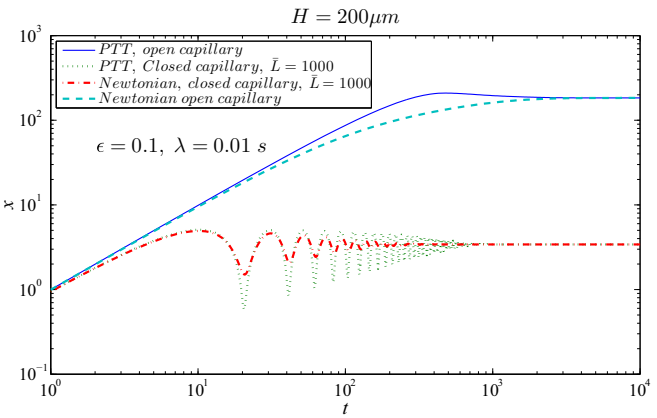

FIG. 4. (Color online) Capillary filling distance as a function of time for the PTT fluid and Newtonian fluid for a closed vertical capillary. The PTT parameters are fixed as $\varepsilon = 0.1$ and $\lambda = 0.01$ s. The channel height is 200 microns and the ratio of the length of the closed capillary to the channel half height is 1000. Density and viscosity of the Newtonian fluid have been taken the same as the PTT fluid (values given at the beginning of this section).

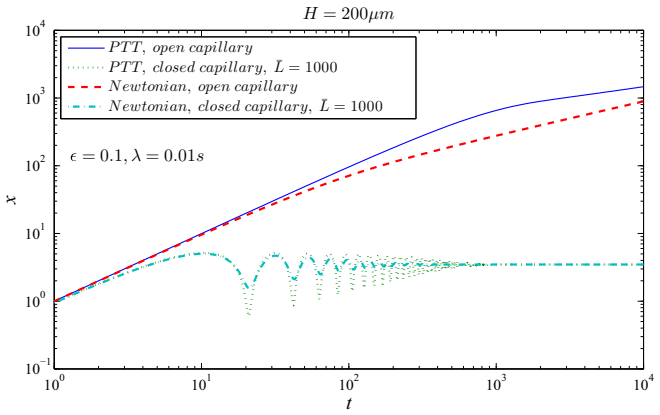

FIG. 5. (Color online) Capillary filling distance as a function of time for the PTT fluid and Newtonian fluid for a closed horizontal capillary. The PTT parameters are fixed as $\varepsilon = 0.1$ and $\lambda = 0.01$ s. The channel height is 200 microns and the ratio of the length of the closed capillary to the channel half height is 1000. Density and viscosity of the Newtonian fluid have been taken the same as the PTT fluid (values given at the beginning of this section).

due to the presence of the retarding pressure from the entrapped gas. However, for open channels, the capillary front keeps on moving forward with an ever decreasing velocity. Subsequently we demonstrate that after a long time, the x versus t curve asymptotically approaches that of a Newtonian fluid, in an open horizontal capillary. Combining Figs. 4 and 5, one can easily infer that the amplitude of the oscillations near the equilibrium position is strongly dependent on fluid rheology. In general, we can conclude that a pure PTT fluid moves faster in a capillary as compared to a Newtonian fluid with the same density and dynamic viscosity. In addition to this, oscillations are expected to occur for PTT fluids as compared to Newtonian fluids at much smaller channel height. We elaborate more on this phenomenon of oscillation in the forthcoming subsection.

C. Linearized analysis: Onset of oscillations

In the previous subsection we have highlighted the essential features of capillary filling for PTT fluids as compared to corresponding Newtonian fluids, with similar dynamical properties. The results of the previous sections demonstrate that onset of oscillation comes very early for PTT fluids, in comparison to the Newtonian ones, for similar channel geometries and fluid properties. Figures 2 and 3 in particular depict that as the fluid properties are made increasingly similar to a Newtonian fluid, the tendency to undergo oscillation near the Jurin height decreases drastically. Additionally, we also note that in cases of closed capillaries the tendency to undergo oscillations increases, even in the absence of gravity, as evident from Figs. 4 and 5 in the previous subsections. In this section we look into the occurrences of oscillations near the Jurin or equilibrium height or length in greater detail. Towards this, we will linearize Eq. (19) around the Jurin or equilibrium length and attempt to pinpoint the cases when oscillations are likely to occur. In this aspect it should be noted that oscillations of capillary front near and around the Jurin height have previously been verified experimentally [45], albeit for Newtonian fluids. Recently, the issue of capillary oscillations was addressed from a theoretical perspective and the necessary conditions for oscillations were specified in terms of the ratio of Bond number ($\mathrm{Bo} = \rho g H^2/\gamma_s$) and Ohnesorge number ($\mathrm{Oh} = \sqrt{\eta/\rho\gamma_s H}$) [46]. Here, we undertake a more quantitative approach to point out the regimes of oscillations from the governing equation itself.

We first find out the Jurin height for the front, when entrapped air is present. Towards this, we first write the main governing equation (19) in the following form:

$$\frac{d}{d\bar{t}}\left[(\bar{x})\frac{d\bar{x}}{d\bar{t}}\right] = \cos\theta - A\bar{x}\bar{h}\left(\frac{d\bar{x}}{d\bar{t}}\right) - B\bar{x} - C\left(\frac{\bar{x}}{\bar{L}-\bar{x}}\right). \tag{21}$$

In Eq. (21), $A = 2\eta\beta/\gamma_s$, $B = \rho g H^2/\gamma_s$, and $C = p_0 H/\gamma_s$. Now, the Jurin height can be very easily evaluated by equating $d\bar{x}/d\bar{t}$ and $d^2\bar{x}/d\bar{t}^2$ to zero in Eq. (21). This results in a quadratic equation in $\bar{J}$ (Jurin height); however, since $\bar{J}$ has to be less than $\bar{L}$, we get the corresponding Jurin height as

$$\bar{J} = \frac{B\bar{L} + \cos\theta + C - \sqrt{(B\bar{L} + \cos\theta + C)^2 - 4B\bar{L}\cos\theta}}{2B}. \tag{22}$$

In the absence of gravity, i.e., in a horizontal channel, the Jurin length becomes [putting $B = 0$ in Eq. (21)]

$$\bar{J} = \frac{\bar{L}\cos\theta}{C + \cos\theta}. \tag{23}$$

Here, we recast Eq. (21) in terms of another coordinate $\tilde{x} = \bar{J} - \bar{x}$, which essentially measures the distance of the capillary from the equilibrium height. We additionally assume that $\tilde{x}/\bar{J} \ll 1$ and $\frac{d\tilde{x}}{d\bar{t}} \ll 1$ so that we can neglect the nonlinear terms involving $\tilde{x}$. In the same spirit we also linearize any power series involving $\tilde{x}$ or $d\tilde{x}/d\bar{t}$ using the approximation: $(1+z)^n \sim 1 + nz \;\forall\, z \ll 1$. Quite intuitively, this approximation is used in linearizing the terms involving viscous resistance and force exerted by the entrapped gas. Enforcing the linearization scheme, we finally obtain an equation for $x_1 = \tilde{x}/\bar{J}$ (i.e., we have rescaled $\tilde{x}$), which reads

$$\frac{d^2x_1}{dt^2} + \frac{3A}{2}\frac{dx_1}{dt} + \left[\frac{B}{\bar{J}} + \frac{C\bar{L}}{\bar{J}(\bar{L}-\bar{J})^2}\right]x_1 = 0. \tag{24}$$

This is an equation for damped oscillation, with natural frequency $\omega = \sqrt{\frac{B}{\bar{J}} + \frac{C\bar{L}}{\bar{J}(\bar{L}-\bar{J})^2}}$. Since A denotes the strength of viscous forces, it is quite intuitive that for strong viscous forces, the system will be overdamped and there will be no oscillations or overshooting near the Jurin height. Assuming a solution of the type $x_1 = \exp(m\bar{t})$, it follows that

$$m = \frac{-\alpha \pm \sqrt{\alpha^2 - 4\omega^2}}{2}, \tag{25}$$

where $\alpha = 3A/2$. Equation (25) clearly predicts that there will be oscillations, when $\alpha^2 - 4\omega^2 < 0$ and in cases of $\alpha^2 - 4\omega^2 > 0$, the capillary will reach the equilibrium height without any oscillations. In the absence of any entrapped air, i.e., for open capillaries, the condition for oscillations to occur

thus turns out to be

$$H > \left(\frac{9\eta^2\gamma_s\cos\theta}{4\rho^3 g^2}\right)^{1/5}. \tag{26}$$

When entrapped gases are present in the channel, the corresponding condition, however, becomes algebraically involved. There are several other interesting points to note from Eq. (24). Firstly, the effects of rheology are absent in the equation, which suggests that the oscillations near the Jurin height are rheology independent, which, of course, is not true as we show subsequently. To be more specific, this equation is identical to that obtained for a Newtonian fluid, near the Jurin height (this can be verified by applying the same procedure to the Lucas-Washburn equation). This is understandable, since for typically low velocities, signified by the assumption $d\bar{x}/d\bar{t} \ll 1$, i.e., for low shear rates, viscoelastic fluids behave similarly to Newtonian fluids, which is the genesis of Eq. (24). Therefore, the preceding analysis can be predicted to hold well for Newtonian fluid, although for PTT fluids, this simple equation perhaps cannot capture the phenomenon of oscillations. To verify this, we first do a simple test for the Newtonian model, with $H = 260\ \mu$m ($\alpha^2 - 4\omega^2 = 1.41 \times 10^{-4} > 0$) and 400 μm ($\alpha^2 - 4\omega^2 = -0.0016 < 0$) and plot x versus t in Fig. 6(a). We clearly observe that for the cases of $H = 260\ \mu$m, no oscillations occur, whereas oscillations are witnessed for $H = 400\ \mu$m. This is clearly in accordance with the predictions of our linearized equations. In Fig. 6(b) we do a similar test for a PTT and a Newtonian fluid, for $H = 270\ \mu$m, for which $\alpha^2 - 4\omega^2 = 3 \times 10^{-5} > 0$. Here, we see that although for Newtonian fluid no oscillations are observed, which is in accordance with the linear analysis, overshooting and oscillations are observed for PTT fluid, which does not follow the present linear theory. This phenomenon underlines the importance of rheology in the capillary dynamics, which dictates the occurrence of oscillations through the nonlinear terms in the viscous resistance force, which we have neglected in deriving Eq. (24). Quite intuitively the aforementioned departure from the linear model is more when the parameter σ which is dictated by the values of relaxation time and elongational parameter is higher.

The second major implication of Eq. (24) is that the natural frequency increases when entrapped air is present in the channel, as evident from the expression of ω mentioned previously. It also becomes apparent from the linear analysis that entrapped air helps in triggering oscillations in the capillary filling, by increasing the value of ω. In addition to this, we can also infer that the natural frequencies of oscillation for both PTT and Newtonian fluids are the same, as predicted by the linear analysis. All these predictions are confirmed in Figs. 4 and 5, where we clearly witness the occurrence of oscillations when entrapped air is present, whereas no oscillations occur in cases of open capillary, both with and without gravity (of course, without gravity oscillations will never occur). Therefore, in conclusion we can infer that the linearized equations offer a good qualitative estimate of the behavior of the capillary front near the Jurin height, for both closed and open capillaries. However, when dealing with PTT fluids, the present simple linear analysis fails to predict the occurrence of oscillations, thus underlining the influence of rheology in the process.

D. Scaling estimates: Role of rheology

In an effort to pinpoint the implications of fluid rheology on capillary dynamics as evident from Figs. 2 and 3, we attempt

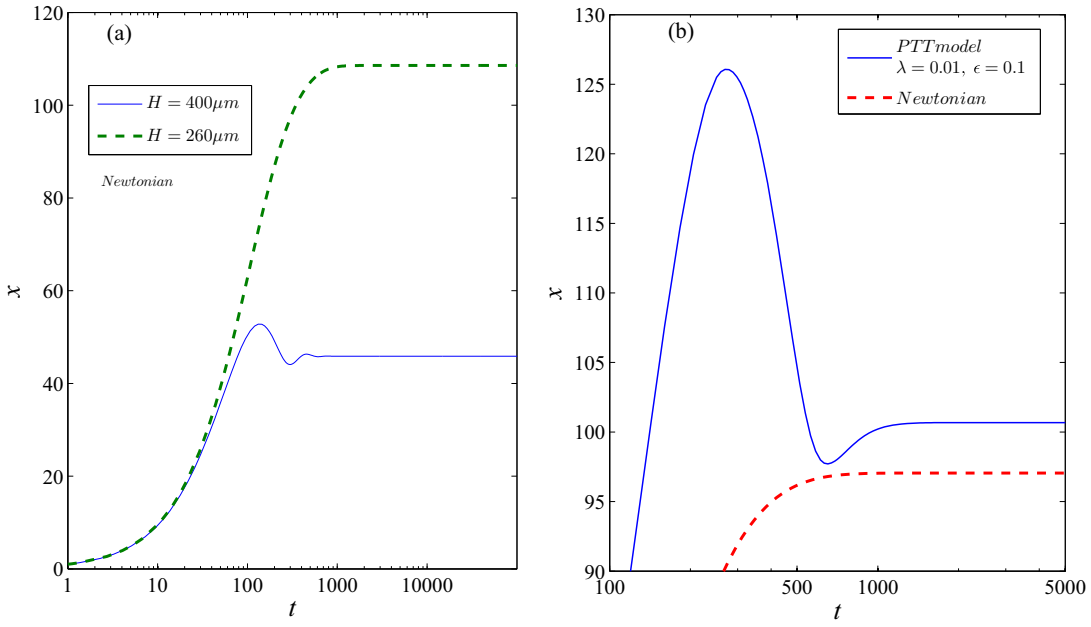

FIG. 6. (Color online) (a) Variation of capillary penetration distance as a function of time for two different channel heights of 400 and 260 microns. (b) Variation of the capillary penetration distance as a function of time for PTT ($\varepsilon = 0.1$, $\lambda = 0.01$ s) and Newtonian fluid in horizontal channels without entrapped air. Density and viscosity of the Newtonian fluid have been taken the same as the PTT fluid (values given at the beginning of this section).

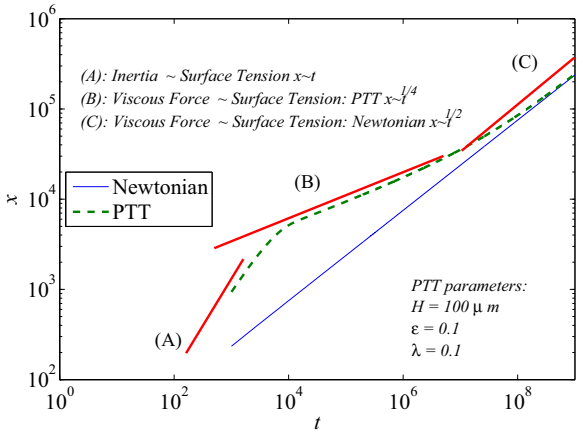

FIG. 7. (Color online) Capillary filling distance as a function of time for PTT fluid ($\varepsilon = 0.1, \lambda = 0.1$ s) and Newtonian fluid depicting the various scaling regimes. Three distinct regimes (A), (B), and (C) are seen for the PTT fluid in contrast to the inertial and Washburn regimes for the Newtonian fluid. The dashed line represents the numerical solution for PTT fluid and the solid line represents the numerical solution for the Newtonian fluid. The red (thick gray) lines depict the scaling solutions. Density and viscosity of the Newtonian fluid have been taken the same as the PTT fluid (values given at the beginning of this section). The height of the capillary $H = 100\ \mu$m.

to shed light on some qualitative aspects of the same through a scaling estimate of the various forces acting on the liquid column. Towards this we note that, in order to demarcate the different scaling regimes, it is better to have sustained capillary filling for a long time. However, considerations of gravity (vertical channels) and entrapped air (closed capillary) lead to onset of oscillations, which we have already discussed in detail in the previous subsection. Further, the motion of the capillary is also not sustained for a long time, when these forces are included in the governing equation. Therefore, we consider the capillary motion in a horizontal channel without the retarding effects of gravity and entrapped air. In the early regime, the motion of the capillary front is driven by the balance of the inertial force and the surface tension force. Clearly, this regime is independent of the fluid rheology and has been previously verified by a number of researchers [45–48]. Therefore, in this regime, one may write $x \sim t$. This can be clearly seen in Fig. 7 where we have depicted the capillary filling distance as a function of time for the PTT fluid and the Newtonian fluid. The regime (A) is the aforementioned linear inviscid regime which is also seen for Newtonian fluid as well (as corroborated from Figs. 2 and 3). As seen from Fig. 7, the linear regime lasts much longer for the PTT fluid than the Newtonian case with a much larger displacement. As time progresses, the viscous forces begin to dominate over the inertial forces. Thus, this regime is a balance of the surface tension force and the inertial force which results in the classical Washburn regime for Newtonian fluids. In stark contrast to the Washburn regime, for the PTT model, we can clearly see a deviation. In order to qualitatively explain this departure from the Washburn regime, we appeal to the viscous stress induced by the PTT fluid on the capillary walls. The shear stress is given by $\tau_{xy} = P_{,x}y$ and the reference velocity is given by $u_{\rm ref} = -\frac{H^2}{2\eta}P_{,x}$ which can be simplified as

$$u_{\rm ref} = \frac{\left[\left(135\bar{u} + 5\sqrt{\frac{40+729\bar{u}^2\sigma}{\sigma}}\right)\sigma^2\right]^{1/3}}{6\sigma} - \frac{5}{3\left[\left(135\bar{u} + 5\sqrt{\frac{40+729\bar{u}^2\sigma}{\sigma}}\right)\sigma^2\right]^{1/3}},$$

as was shown in Sec. II. For the long-time dynamics, for the cases where σ is significant, the first term in $u_{\rm ref}$ plays a dominant role over the second which results in the order of magnitude of $u_{\rm ref}$ as $\bar{u}^{1/3}$. As a consequence of this, one can write the shear stress to be of the order of $\tau_{xy} \sim \bar{u}^{1/3} \sim \frac{x^{1/3}}{t^{1/3}}$ which results in the total viscous force acting on the liquid column as $x\tau_{xy} \sim \frac{x^{4/3}}{t^{1/3}}$. Upon equating this with the surface tension force, we obtain $\gamma_s \sim \frac{x^{4/3}}{t^{1/3}}$ which finally yields the intermediate regime (B) as $x \sim t^{1/4}$. This intermediate 1/4 regime is unique to PTT fluids and is clearly seen in Fig. 7. Far from this intermediate regime, the velocity (and hence the shear rates) become so small that the PTT behavior asymptotically tends to Newtonian behavior and hence the PTT fluid also shows a *delayed* Washburn dynamics for very long times [Regime (C)], where the variation $x \sim \sqrt{t}$ is observed.

IV. CONCLUSIONS

In this work, we have demonstrated the capillary filling for viscoelastic fluids described by the most general constitutive behavior through the framework of the Phan-Thien–Tanner model, for both horizontal and vertical channels. We have demonstrated that the onset of oscillations near the Jurin height occurs in much narrower channels for PTT fluids as compared to Newtonian fluids. We also depicted that in general, for a pure PTT fluid, the capillary filling process is faster as compared to that for a Newtonian fluid. We then proceeded to show the influence of trapped air on the isothermal capillary filling of PTT fluids. Through a linearized analysis we further explained that the presence of entrapped air helps trigger oscillations of the capillary front near the Jurin height. In addition to this, through a scaling estimate we highlight an intermediate 1/4 scaling regime which is a unique hallmark of PTT fluids; this is followed by the classical Washburn regime.

APPENDIX: JUSTIFICATION FOR THE QUASISTEADY UNIDIRECTIONAL FLOW FIELD ASSUMPTION

The approach towards modeling of capillary filling involves three distinct flow regimes—the entry regime, the Poiseuille regime, and the surface traction regime (for a detailed discussion, please see [34,49,50]). Out of these three regimes, the Poiseuille regime is the most dominant regime and hence in such a case, the viscous drag acting on the liquid column is found by considering a *unidirectional steady* flow [see, for example, the seminal works by Lucas and Washburn [51] and the book by Bruus [52], Chap. 7, Sec. 7.3.2, Eq. (7.23)]. This approximation has been widely used in all the literature concerning the capillary filling of Newtonian [51–53] as well as non-Newtonian fluids [34,37,54]. The procedure followed is that the total viscous resistance on the liquid column is proportional to the cross-sectional average steady

state velocity, which is considered to be the velocity of the capillary front.

The average velocity and the viscous stress are found by solving for the steady unidirectional momentum equation for the concerned fluid (Navier-Stokes for the Newtonian case and Cauchy's momentum equation for non-Newtonian cases). A number of previous works have validated this approach with already existing experimental data on capillary filling for various operation conditions [26,33,51,55].

In an effort to delve deeper into such propositions we perform a simple scaling analysis of the governing momentum equations, i.e., the Cauchy's equation of motion. The momentum balance equation, accounting for the temporal term can be written in the following form (assuming u to be a function of y and t):

$$\rho\frac{\partial u}{\partial t} = -\frac{\partial p}{\partial x} + \frac{\partial \tau_{yx}}{\partial y}. \tag{A1}$$

The symbols bear their usual meaning. We now perform a scaling estimate of the various terms in the equation, for the cases of capillary filling and in the process attempt to show that the temporal term is quite small as compared to the viscous term on the right-hand side, as a result of which it can be neglected in evaluation of the viscous stress. Towards this we first note that $\rho\frac{\partial u}{\partial t} \sim \frac{\rho u_f}{t_f}$, where u_f and t_f are characteristic filling velocity and time, respectively. Additionally, we note that $u_f \sim J/t_f$, where J $(=\gamma\cos\theta/\rho g H)$ is the Jurin height or the equilibrium height. Therefore, the temporal term becomes $\rho\frac{\partial u}{\partial t} \sim \frac{\rho J}{t_f^2}$. In a similar way one can scale the viscous term on the right-hand side of Eq. (A1): $\frac{\partial \tau_{yx}}{\partial y} \sim \frac{\mu u_f}{H^2} \sim \frac{\mu J}{H^2 t_f}$, where H is the channel dimension and μ is the viscosity of the fluid. The relative importance of the two terms can be easily evaluated by taking the ratio of the two terms, which comes out to be $\frac{\text{Temporal term}}{\text{Viscous term}} \sim \frac{\rho H^2}{t_f \mu}$. This number is also referred to as the Weissenberg number (or equivalently the time dependent Reynolds number).

We now evaluate the order of magnitude of this term for some typical cases of capillary filling, based on previously reported experimental data on capillary filling and demonstrate that the Weissenberg number is extremely small. Following the seminal work of Quere [45] for the filling of silicone oil the typical time for capillary filling is $\sim O(100)$ s; the properties of silicone oil are $\rho = 980$ kg/m^3, $\mu = 0.5$ Pa s, $J = 10.4$ mm, $\gamma = 0.02116$ N/m, while the channel radius was $R = 421$ μm. Substituting these values in the Weissenberg number, we obtain $\frac{\rho H^2}{t_f \mu} \sim 10^{-6}$. We report another short case study following the experiments of Radiom *et al.* [33], which considers entrapped air in the capillary. In their experiments, a glycerol–de-ionized (DI) water mixture was considered, with varying concentrations of glycerol. For the present purpose, we chose the data set for 80% glycerol-DI water mixture, with the following properties: $\mu = 0.08$ Pa s (calculated from Tables 1 and 3 in Ref. [33]), $\rho = 1208$ kg/m^3, R (channel radius) $= 300$ μm, while the filling time was in the tune of ~0.5–1 s. Putting these values in the Weissenberg number we get $\frac{\rho H^2}{t_f \mu} \sim 10^{-3}$. The two aforementioned sample calculations indeed demonstrate that the temporal term can be safely neglected as compared to the viscous terms, which play a dominant role in dictating the velocity. This implies that the liquid motion can be described by a quasisteady process, wherein the time over which velocity and pressure appreciably change is very slow and therefore, the liquid can instantaneously adjust to the changing pressure gradient.

Assumption of quasisteady state is a widely used approximation for slow movement of liquid, even if the conditions or forces change with time (for example, deformation of drops in creeping flows for low capillary numbers; see Chap. 8, Sec. C in [56], etc). In our present work we have adopted this same approach, where we evaluate the viscous drag on the liquid column, based on the steady state solution of unidirectional Cauchy's momentum equation for a PTT fluid, as outlined in Eqs. (2)–(8) and (11).

[1] H. A. Stone, A. D. Stroock, and A. Ajdari, Annu. Rev. Fluid Mech. **36**, 381 (2004).
[2] S. Haeberle and R. Zengerle, Lab on a Chip **7**, 1094 (2007).
[3] H. J. Keh and H. C. Tseng, J. Colloid Interface Sci. **242**, 450 (2001).
[4] A. E. Herr, J. I. Molho, J. G. Santiago, M. G. Mungal, T. W. Kenny, and M. G. Garguilo, Anal. Chem. **72**, 1053 (2000).
[5] E. D. Torniainen, A. N. Govyadinov, D. P. Markel, and P. E. Kornilovitch, Phys. Fluids **24**, 122003 (2012).
[6] Z. Yin and A. Prosperetti, J. Micromech. Microeng. **15**, 643 (2005).
[7] Z. Yin and A. Prosperetti, J. Micromech. Microeng. **15**, 1683 (2005).
[8] D. Juncker, H. Schmid, U. Drechsler, H. Wolf, M. Wolf, B. Michel, N. de Rooij, and E. Delamarche, Anal. Chem. **74**, 6139 (2002).
[9] G. M. Walker and D. J. Beebe, Lab on a Chip **2**, 131 (2002).
[10] T. Vestad, D. W. M. Marr, and J. Oakey, J. Micromech. Microeng. **14**, 1503 (2004).
[11] J. W. Suk and J.-H. Cho, J. Micromech. Microeng. **17**, N11 (2007).
[12] M. Zimmermann, H. Schmid, P. Hunziker, and E. Delamarche, Lab on a Chip **7**, 119 (2007).
[13] M. Zimmermann, P. Hunziker, and E. Delamarche, Microfluid. Nanofluid. **5**, 395 (2008).
[14] M. Zimmermann, P. Hunziker, and E. Delamarche, Biomed. Microdevices **11**, 1 (2009).
[15] J. C. T. Eijkel and A. van den Berg, Lab on a Chip **6**, 1405 (2006).
[16] N. Srivastava and M. A. Burns, Anal. Chem. **78**, 1690 (2006).
[17] S. Chibbaro, Eur. Phys. J. E **27**, 99 (2008).
[18] F. Diotallevi, L. Biferale, S. Chibbaro, G. Pontrelli, F. Toschi, and S. Succi, Eur. Phys. J. Spec. Top. **171**, 237 (2009).
[19] A. A. Saha and S. K. Mitra, J. Fluids Eng. **131**, 061202 (2009).
[20] P. K. Mondal, U. Ghosh, A. Bandopadhyay, D. DasGupta, and S. Chakraborty, Phys. Rev. E **88**, 023022 (2013).

[21] J. Haneveld, N. R. Tas, N. Brunets, H. V. Jansen, and M. Elwenspoek, J. Appl. Phys. **104**, 014309 (2008).
[22] M. Dreyer, A. Delgado, and H.-J. Path, J. Colloid Interface Sci. **163**, 158 (1994).
[23] P. Mandal, R. Dey, and S. Chakraborty, Lab on a Chip **12**, 4026 (2012).
[24] J. W. van Honschoten, N. Brunets, and N. R. Tas, Chem. Soc. Rev. **39**, 1096 (2010).
[25] S. Levine, J. Lowndes, E. J. Watson, and G. Neale, J. Colloid Interface Sci. **73**, 136 (1980).
[26] Y. Xiao, F. Yang, and R. Pitchumani, J. Colloid Interface Sci. **298**, 880 (2006).
[27] V.-N. Phan, C. Yang, and N.-T. Nguyen, Microfluid. Nanofluid. **7**, 519 (2009).
[28] P. R. Waghmare and S. K. Mitra, Microfluid. Nanofluid. **12**, 53 (2011).
[29] D. Dimitrov, A. Milchev, and K. Binder, Phys. Rev. Lett. **99**, 054501 (2007).
[30] C. Bakli and S. Chakraborty, Appl. Phys. Lett. **101**, 153112 (2012).
[31] C. Bakli and S. Chakraborty, J. Chem. Phys. **138**, 054504 (2013).
[32] V. N. Phan, N.-T. Nguyen, C. Yang, P. Joseph, L. Djeghlaf, D. Bourrier, and A.-M. Gue, Langmuir **26**, 13251 (2010).
[33] M. Radiom, W. K. Chan, and C. Yang, Microfluid. Nanofluid. **9**, 65 (2009).
[34] S. Chakraborty, Anal. Chim. Acta **605**, 175 (2007).
[35] P. C. Sousa, F. T. Pinho, M. S. N. Oliveira, and M. A. Alves, Biomicrofluidics **5**, 014108 (2011).
[36] M. L. Olivares, L. Vera-Candioti, and C. L. A. Berli, Electrophoresis **30**, 921 (2009).
[37] K. G. Kornev and A. V. Neimark, J. Colloid Interface Sci. **262**, 253 (2003).
[38] N. P. Thien and R. I. Tanner, J. Non-Newtonian Fluid Mech. **2**, 353 (1977).
[39] F. T. Akyildiz, Int. J. Eng. Sci. **40**, 859 (2002).
[40] G. B. Thurston, Biophys. J. **12**, 1205 (1972).
[41] T. Hayat, S. Noreen, and A. A. Hendi, J. Biorheol. **25**, 8 (2011).
[42] J. S. Field, M. V. Swain, and N. Phan-Thien, J. Non-Newtonian Fluid Mech. **65**, 177 (1996).
[43] Y. Fan, R. I. Tanner, and N. Phan-Thien, J. Non-Newtonian Fluid Mech. **84**, 233 (1999).
[44] P. J. Oliveira and F. T. Pinho, J. Fluid Mech. **387**, 271 (1999).
[45] D. Quéré, Europhys. Lett. **39**, 533 (1997).
[46] S. Das, P. R. Waghmare, and S. K. Mitra, Phys. Rev. E **86**, 067301 (2012).
[47] M. Stange, M. E. Dreyer, and H. J. Rath, Phys. Fluids **15**, 2587 (2003).
[48] F. Maggi and F. Alonso-Marroquin, Phys. Rev. E **88**, 053013 (2013).
[49] W. Huang, R. S. Bhullar, and Y. C. Fung, Trans. ASME **123**, 446 (2001); H. S. Lew and Y. C. Fung, J. Biomech. **3**, 23 (1970).
[50] S. Chakraborty, *Microfluidics and Microfabrication* (Springer, New York, 2010).
[51] R. Lucas, Kolloid Z. **23**, 15 (1918); E. W. Washburn, Phys. Rev. **17**, 273 (1921).
[52] H. Bruus, *Theoretical Microfluidics* (Oxford University Press, Oxford, 2008).
[53] J. A. Thomas, M. P. Boyle, L. W. Hunter, and J. E. Tiffany, J. Colloid Interface Sci. **372**, 176 (2012); R. Chebbi, *ibid.* **315**, 255 (2007); Guy Ramon and Alexander Oron, *ibid.* **327**, 145 (2008); C. P. Tso and K. Sundaravadivelu, J. Phys. D **34**, 3522 (2001).
[54] R. M. Digilov, Langmuir **24**, 13663 (2008); S. Chakraborty, Lab Chip **5**, 421 (2005).
[55] M. Hultmark, J. M. Aristoff, and H. A. Stone, J. Fluid Mech. **678**, 600 (2011); N. Ichikawa, K. Hosokawa, and R. Maeda, J. Colloid Interface Sci. **280**, 155 (2004); N. Ichikawa and Y. Satoda, *ibid.* **162**, 350 (1994); S. Das and S. K. Mitra, Phys. Rev. E **87**, 063005 (2013).
[56] L. G. Leal, *Advanced Transport Phenomena* (Cambridge University Press, New York, 2007).